[3]H. Tai, R. Bassel, E. Gerjuoy, and V. Franco, Phys. Rev. (to be published).

[4]D. M. Chase, Phys. Rev. 104, 838 (1956).

[5]M. Mittleman, J. Peacher, and B. Rozsnyai, Phys. Rev. 176, 180 (1968).

[6]L. L. Foldy and J. D. Walecka, Ann. Phys. (N. Y.) 54, 447 (1969).

[7]R. J. Glauber, in *Lectures in Theoretical Physics*, edited by W. E. Brittin and L. G. Dunham (Interscience New York, 1959), Vol. I.

[8]M. H. Mittleman and K. M. Watson, Ann. Phys. (N. Y.) 10, 268 (1960).

[9]G. Takeda and K. M. Watson, Phys. Rev. 97, 1336 (1955).

[10]H. Feshbach, Ann. Phys. (N.Y.) 19, 287 (1962).

[11]This result may also be obtained as a second-order approximation to the equivalent potential, as was shown in Ref. 12.

[12]M. H. Mittleman, Ann. Phys. (N.Y.) 14, 94 (1961).

[13]Recently, H. Feshbach and J. Hüfner [Ann. Phys. (N.Y.), 56 269 (1969)] have suggested an equation similar to (8) and have used a similar completeness approach to the evaluation of the last term. They also use the one average elastic channel idea proposed here.

[14]Actually, (9) is expressible in Lommel functions, but this is here termed "not analytically obtainable."

[15]L. Vriens, C. Kuyatt, and S. Mielczarek, Phys. Ref. 170, 163 (1968).

[16]R. L. Sugar and R. Blankenbeder, Phys. Rev. 183, 1387 (1969); D. S. Saxon and L. I. Schiff, Nuovo Cimento 6, 614 (1957); M. Levy and J. Sucher, Phys. Rev. (to be published).

PHYSICAL REVIEW A VOLUME 2, NUMBER 5 NOVEMBER 1970

Single-Electron Capture by C^{4+} in Helium, Neon, and Argon below 40 keV*

H. Jay Zwally and David W. Koopman

Institute for Fluid Dynamics and Applied Mathematics, University of Maryland, College Park, Maryland 20742

(Received 27 March 1970)

Total cross sections for single-electron capture by C^{4+} from the target gases He, Ne, and Ar were measured at laboratory energies between 400 eV and 40 keV. The fast-collision products that scattered less than 1° were charge analyzed after single collision in a gas cell. Experimental results are interpreted in terms of pseudocrossings of the adiabatic potential curves for the initial and final states. The cross sections for $C^{4+}+He$ and $C^{4+}+Ne$ are consistent with the second maximum predicted for distant pseudocrossings by a numerical solution of the two-state semiclassical approximation by Bates, Johnson, and Stewart. Electron capture with an Auger-type ionization of the target is exothermic for $C^{4+}+Ne$ and $C^{4+}+Ar$ and is considered as the explanation of the large (50 Å^2) and slowly varying cross section measured for $C^{4+}+Ar$.

I. INTRODUCTION

Low-velocity collisions between heavy particles frequently are described by the adiabatic potential-energy curves of the quasimolecule formed by the colliding atoms. The adiabatic description is appropriate when the relative velocity (V_R) of approach is small compared to the orbital velocity of internal electron motion. An electron transfer between collision partners is viewed in this model as a transition between states of the quasimolecule in a region of internuclear separation (R) where the adiabatic potential curves for the states are sufficiently close for an appreciable transition probability to exist. Collisions of multiply charged ions with neutral atoms are particularly interesting because the phenomenon of pseudocrossing of the adiabatic potential-energy curves significantly effects the transition probability.

The dominant process in multiply charged ion-atom collisions is usually single-electron capture, e.g.,

$$C^{4+}+He \rightarrow C^{3+}+He^{+}+\Delta E_i \ , \qquad (1.1)$$

where ΔE_i is the energy defect between the ith pair of initial and final states at infinite R. In the present experiment, a beam of C^{4+} ions was directed through a thin gas target under single-collision conditions, and the fast-collision products were separated and measured according to their charge. The ratio of C^{3+} to incident C^{4+} (ground state) provided the total cross section for single-electron capture without regard for the excitation state of the products. Since the relative collisions velocities were in the range of $(1-8)\times10^7$ cm/sec, consideration of the adiabatic curves is appropriate. [For a carbon projectile, we have $E_{lab}^{1/2}=25.2V_R$, where E_{lab} is in eV, and V_R in units of 10^7 cm/sec.]

Potential-energy curves for process (1.1) that include only the target polarization in the initial state and the Coulomb repulsion in the final state are good classical approximations for $R \gtrsim 2.5a_0$. If ΔE is positive (exothermic) and the states have the same symmetry, their adiabatic potential curves

pseudocross[1] at some R_x. The well-known Landau-Zener (LZ) approximation for the transition probability in the pseudocrossing region has given a semiquantative description of capture cross sections for some systems with moderate R_x ($3.5a_0 \leq R_x \leq 6a_0$).[2,3]

In 1960, Bates[4] criticized the LZ treatment for several reasons, including the assumption that transitions occur only in a narrow ill-defined region around the pseudocrossing. A recent paper by Heinrichs[5] reviews extensive theoretical modifications to the original LZ treatment and present corrections to that approximation. Heinrichs also gives a new definition for the width of the transition region and discusses the validity of the LZ theory as a zeroth-order approximation. Simple consideration of the separation between potential-energy curves supports Bates's conclusion that transitions may readily occur well away from the crossing. Since the separation at the crossing relative to the separation away from the crossing depends on the magnitude of R_x, the relative importance of transitions away from the crossing is also dependent on R_x. To facilitate discussion, we define three regions of R_x as close, distant, or moderate, accordingly, as R_x is less than $3.5a_0$, greater than $8a_0$, or between these values. A recent numerical solution by Bates, Johnson, and Stewart[6] (BJS) of the two-state semiclassical approximation, which includes contributions to the transition probability throughout the interaction region, gives significant deviations from the simpler LZ solution. In particular, the BJS solution for a system ($Mg^{2+} + H \rightarrow Mg^{+} + H^{+}$, $R_x = 18.9a_0$) with a distant crossing gives a second maximum in the total cross section at higher velocity than the ordinary LZ maximum.

Total cross sections for electron capture are in effect measurements of the transition probability as a function of relative velocity, integrated over the impact parameter. Additional experimental results that can be ascribed to specific pseudocrossing states are required to explore the validity of various treatments of the pseudocrossing problem. Our present results are a step in this direction. The combinations of C^{4+} with He and Ne both have very close ($R_x \approx 2.5a_0$) pseudocrossings for capture into the ground $2s$ (or $2p$) state of C^{3+}, and very distant ($R_x \gtrsim 35a_0$ for He and $R_x \gtrsim 15a_0$ for Ne) crossings for capture into the $3s$ (or $3p$) state. Our interpretation is that these measured cross sections are primarily due to single-electron capture into the states having distant crossings as described by the BJS second maximum. In contrast, the respective curves for $C^{4+} + Ar$ cross at moderate separations. However, the two-electron process of capture ionization

$$C^{4+} + Ar \rightarrow C^{3+} + Ar^{2+} + e + 21.1 \text{ eV} , \qquad (1.2)$$

which also can be interpreted in terms of potential-energy curves, is the most plausible explanation of these experimental results.

II. EXPERIMENTAL APPARATUS

Previous cross-section measurements have been restricted to multiply charged ions that could be produced with sufficient intensity in electron bombardment ion sources (e.g., O^{2+}, Kr^{4+}, Ne^{4+}). In order to study systems with less ambiguity of initial and final states, a source of multiply charged ions was developed,[7] in which the ions were extracted from a pulsed plasma formed by an electrical spark. Each pulse of extracted ions was about 2 μsec in duration, and, typically, 10^3–10^5 ions passed through the collision region. The techniques required to measure cross sections using this source are described below and in more detail elsewhere.[8] The apparatus is shown in Fig. 1. A desired ion species was selected from the ion-source output by a double-focusing mass spectrometer (MS) with a mass resolution of 1 per 100 and an energy selection of 4%. A target gas was contained in a small gas cell behind the MS exit slit. After pass-

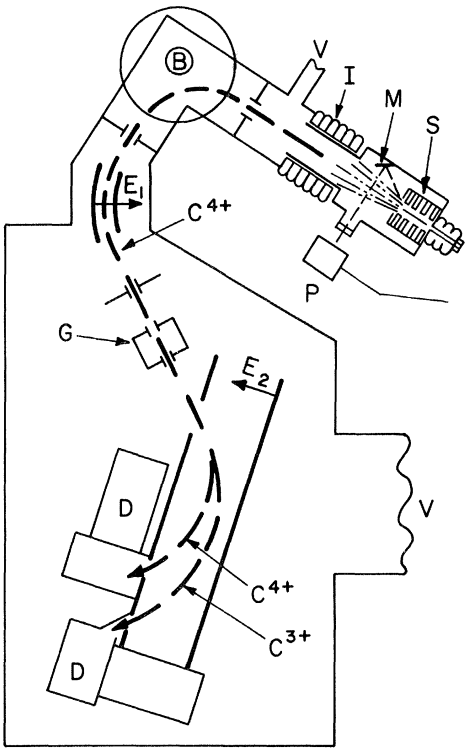

FIG. 1. Diagram of apparatus: S, spark ion source; M, mirror; P, photomultiplier for triggering instrumentation; I, insulation between source and chamber; V, vacuum pump ports; B, magnetic field for momentum selection; E_1 and E_2, electric fields for E/Z selection before and after the collision; G, gas cell; and D, secondary emission detectors.

ing through the target gas, the ion beam was separated by charge state, and the intensities of the primary and secondary ions were simultaneously detected by dual secondary-emission detectors.

The total cross section for electron capture is a simple function of the measured ion intensities provided that the ions are collected and detected in a sufficiently large "cone" about the forward direction. For each azimuthal direction, the maximum angle through which a particle may scatter and be detected is a function of the following: the point of scattering, beam divergence, cell-exit slit size, cell length, the aperture size and location of the separator-detector assembly, the beam energy spread, and the relative change in kinetic energy during a collision. An analysis of these parameters was made[8] with the conclusion that all ions that scatter less than 1° were detected, as well as many ions that scatter to larger angles. Dimensions of the slits and distances between them are given in Table I.

The MS was designed according to the ion-optic equations derived by Mattauch and Herzog.[9] The chosen deflections are 90° in the magnetic sector and 60° in the electric sector, and the respective radii are 6.3 and 8.4 cm. Optimum slit positions were determined by an empirical investigation of the directional focusing properties, and a maximum mass resolution of 1000 was achieved. Precision-machined parts provided accurate alignment of the slits and the fields. The field-regulated magnet[10] was calibrated (to ±0.1% accuracy) as a function of mass and energy, so that the electric and magnetic fields could be preset for a particular mass peak at a given energy. Thus, visual tuning for a peak, which would have been difficult and unreliable because of the pulse to pulse variations in the ion current, was avoided. The MS calibration and other system tests were performed with a steady ion beam from an electron bombardment source.

TABLE I. Slit dimensions in cm.

Location	Width	Height	Distance to next slit
Source exit	1.27 diam		45.7
Baffle	0.318	1.27	1.1
MS input	0.0630	0.635	5.08
input	0.0259	0.635	21.9
intermediate	0.2461	0.635	23.0
output	0.0409	0.635	6.35
Gas cell			
entrance	0.0254	0.635	1.27
exit	0.0787	0.635	5.08
Charge separator			
entrance	1.40	1.27	or 36.9 / 49.2
exit	1.27	1.59	0
Detector	1.27	1.59	

Gas flowed into the cell through a 1.3-cm tube perpendicular to the beam. Another 1.3-cm tube led to a closed volume containing a Millitor ionization gauge[11] and a capacitance manometer.[12] Plates containing the cell slits were mounted on precision rods; Viton O-rings formed the seal between the plates and the cell body. A 1.27-cm extension block could be mounted between the entrance plate and the cell body to double the cell length.

A 45° electrostatic analyzer separated the $z=4$ and $z=3$ charges into two detectors at three and four units from its entrance slit. The entrance was covered with a 95% transparent tungsten grid that eliminated the beam divergence caused by the fringing field of an uncovered slit. Five vertical parallel plates formed the linear electric field. A converging effect in the vertical plane was added by placing horizontal plates above and below the vertical plates at the same potential as the endplate. The energy bandwidth was 5.3% (7%) for the $z=3$ ($z=4$) position; these values were experimentally verified, and the optimum central voltage required for each energy was determined.

The ion detectors were of the Daly secondary-emission type. The instantaneous ion currents were too high for counting techniques and too low (especially the secondary component) for electrometer measurement. Our method obtained a signal from a photomultiplier dynode that had a height proportional to the integrated number of incident ions. The decay time of this dynode signal was long compared to the ion arrival time, and the maximum signal height was measured by a peak-reading memory voltmeter.[13] The dynode signal was calibrated by using a continuous low-intensity beam of ions, which was countable on the dynode and the anode, to determine the mean dynode pulse height per single ion. Calibrations for various ions and charge states were extrapolated to obtain the relative detector sensitivities for the C^{3+} and C^{4+} ions produced only in pulses. The detector design and calibration are described in detail elsewhere.[14]

The base pressure in the vacuum chamber was 5×10^{-8} Torr, which increased as a linear function of the gas cell pressure in the ratio of 1 per 100 (for the slit sizes given in Table I). The ion-source section was differentially pumped to remove the gases produced by the pulsed source.

III. MEASUREMENT PROCEDURE

If the initial component ($z=4$) of the beam can change to only one other component ($z=3$), the cross section, assuming only single collisions, is

$$\sigma_{43}=(NL)^{-1}\ln(I_3/I_0)\ , \qquad (3.1)$$

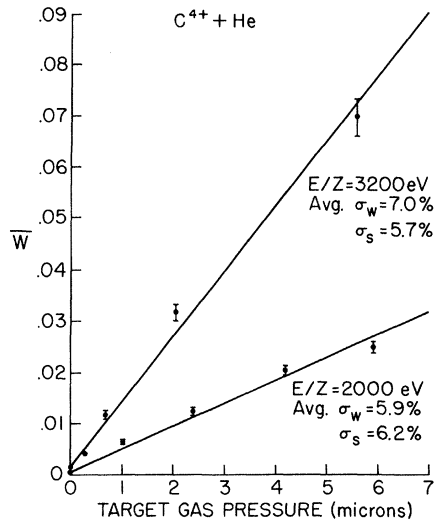

FIG. 2. Average (over 20 pulses of source) of logarithm of ratio of C^{3+} to incident C^{4+} versus target pressure. Error bars represent standard deviation σ_W of measured mean. Standard deviation of slope is σ_s.

where I_3 is the intensity of the $z=3$ component after passage through a target of density N and length L, and $I_0 = I_3 + I_4$ is the incident intensity. Measurements were taken at sufficiently low N for multiple collisions to be negligible, so that Eq. (3.1) is a good approximation. If there are other components k, the approximation is still good provided $I_3 \gtrsim I_k \ll I_0$.

Variations in the measured value of the intensity ratio I_3/I_0 occurred because the number of secondary ions was usually statistically small and possibly because of fluctuations in target gas density from pulse to pulse of the ion source. Data were taken to obtain the quantity

$$W = \ln\left(\frac{I_3}{I_3+I_4}\right) = \sum_{n=1}^{\infty} \frac{1}{n}\left(\frac{I_3}{I_3+I_4}\right)^n \qquad (3.2)$$

for approximately 20 pulses at each of five values of N. The average W at each N is defined as $\overline{W}$; the standard deviation σ_W of the measured mean $\overline{W}$ is typically 7%. The measured $\overline{W}$ versus pressure for process (1.1) at two energies are shown in Fig. 2 with error bars at $\overline{W} \pm \sigma_W$. The straight line is a least-squares linear-curve fit with each point weighted in inverse proportion to $\overline{W}$. This weighting considers the squared deviation at each point in a relative sense and tends to force the line through the small value of $\overline{W}$ at the base pressure. Values of $\overline{W}$ up to 0.2 were included; however, these higher-pressure points, where multiple collisions might be significant, have small weights in the curve fit.

The cross sections, as usual, are proportional to the slopes in Fig. 2. The standard deviation (in a mean sense) of the fitted slope, defined as σ_s, is a measure of the probable cross-section error caused by statistical deviations of the measured $\overline{W}$ from their true mean values as indicated by σ_W, and also by any inherent nonlinearity of the true mean values caused by multiple collisions. The values of σ_s are approximately equal to the respective average σ_W; this comparison provides a test of the single-collision assumption. A plot of $\overline{W}$ versus pressure was made by computer routine at each energy and scanned for linearity. The respective values of the average σ_W and of σ_s were 5.9% and 6.2% at 2000 eV/z; 5.7% and 7.0% at 3200 eV/z. Cross sections are plotted as a function of relative velocity with error bars equivalent to $\pm\sigma_s$.

The effusion of the target gas through the entrance and exit slits of the gas cell causes the effective length L of the target to be longer than the physical length l of the cell. Expressing this end effect as an additive factor gives $L = l + l_e$. Measurement of W at two values of the cell length, $l_1 = 1.27$ cm and $l_2 = 2.54$ cm, with the slit widths given in Table I gives the end correction

$$l_e = (W_1 l_2 - W_2 l_1)/(W_2 - W_1) = 0.16 \ . \qquad (3.3)$$

This was done for single-electron capture by Kr^{3+} + He and C^{2+} + Ar at several energies. The estimated accuracy of the measured l_e is ±10% and corresponds to ±3% error in the measured cross section, since l_e is 32% of l.

The magnetic shielding around the photomultiplier tubes of the detectors proved effective against the fringing field from the mass spectrometer. To test the limit of shielding, a light source was directed into the detectors and produced a constant pulse-count rate up to 9 kG, above which the fringing field increased sharply as evidenced by the departure from linearity of the magnet current versus magnetic field. The magnetic field used for the cross-section measurements was always less than 5 kG.

Data were taken at approximately five velocities a day, and some of the scatter in the cross sections may have been caused by variations in the relative detector gain, which was calibrated four times. Five of the He points and four of the Ne points (labeled x) were obtained when the gain was uncertain; these nine points have been normalized by the same factor. The order of data taking was nearly random, so that unnoted systematic changes in the calibration factor are unlikely.

The ionization gauge was calibrated after each daily run against the capacitance manometer which was factory calibrated and compared with a McLeod gauge in our laboratory. The factor, McLeod/manometer = 0.94, obtained for argon agrees with Utterback and Griffith's[15] valve.

An estimate of the combined limit of error is taken as a simple sum of the limits of each component. The separate limits are gas cell end correction, ± 3%; pressure calibration, ± 2%; detector relative gain calibration, ± 7%; and voltmeter-preamplifier calibration, ±3%. This total estimated limit of error on the absolute cross section of ± 15% is in addition to the scatter indicated by σ_s (typically 7%) and is not included in the cross-section error bars.

IV. LANDAU-ZENER CROSS-SECTION FUNCTION

A cross section based on the LZ formula can be readily calculated from the form of the initial and final diabatic potential-energy curves U_i^0 and U_f^0, respectively, and from the separation ΔU_x of the noncrossing adiabatic potential curves at the crossing R_x. The required formulas, taken from Bates and Moiseiwitsch, [16] are outlined below. The value of ΔU_x from the two-state approximation is a function of matrix elements between the initial and final states and has been calculated[16–20] for a number of specific systems using appropriate wave functions. From these calculations, which were made for systems having R_x between $3.3a_0$ and $20.2a_0$, a rough relationship between ΔU_x and R_x was noted. [20] Hasted and Chong[2] determined some additional values of ΔU_x from their experimental data. We define $\Delta U_x(R_x)$ to be the smooth curve drawn by Hasted and Chong, extrapolate it to smaller and larger R_x, and use this $\Delta U_x(R_x)$ to calculate a cross section defined as σ^{LZ}.

The probability of an ultimate transition between the adiabatic noncrossing potential curves is given by the LZ formula: $P_{nm} = 2P(1-P)$, where $P = e^{-w}$ is the probability of remaining on a diabatic curve at each crossing, and

$$w = \frac{\pi}{2\hbar V_R(R_x)} \left(\frac{\Delta U_x^2}{\left| (d/dR)(U_i^0 - U_f^0) \right|_{R_x}} \right) , \qquad (4.1)$$

where $V_R(R_x)$ is the relative velocity at R_x. Using the R^{-4} polarization and the R^{-1} Coulomb terms in U_i^0 and U_f^0, respectively, gives

$$\left| \frac{d}{dR}(U_i^0 - U_f^0) \right|_{R_x} = \frac{\Delta E^2}{e^2(z-1)} (1+\mu) , \qquad (4.2)$$

where z is the projectile charge and μ is zero if the polarization is neglected. Integration of P_{nm} over impact parameter according to Bates and Moiseiwitsch gives

$$\sigma_{nm}^{LZ} = \pi R_x^2 P(\eta)[(1+\lambda)p] , \qquad (4.3)$$

where $P(\eta)$ is four times an integral calculated by Moiseiwitsch[21] and has a maximum of 0.45 at $\eta = 0.424$; p is the probability that the system approaches on a specified curve and in this experiment, $p = 1$; λ is of order zero, except for very low velocities; and

$$\eta = 247.2 \left(\frac{\sqrt{2}}{(z-1)V_R} \right) \left(\frac{\Delta U_x}{\Delta E/(z-1)} \right)^2 \times (1+\mu)^{-1}(1+\lambda)^{-1/2} . \qquad (4.4)$$

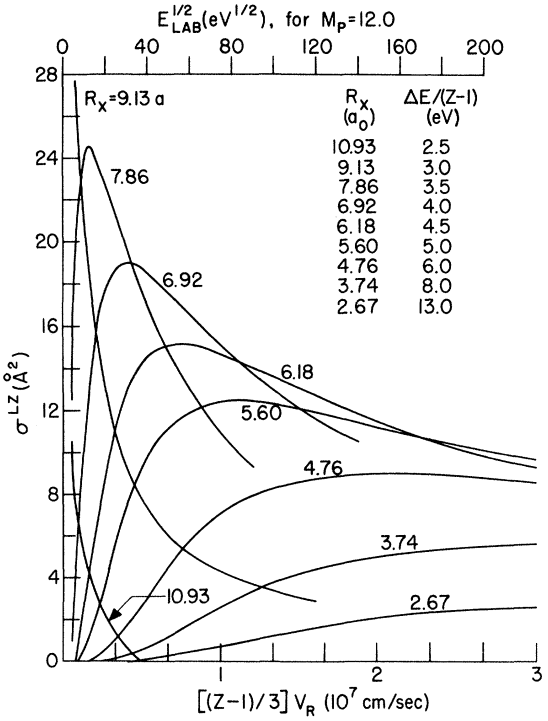

FIG. 3. Landau-Zener cross sections using approximate dependency of ΔU_x on R_x.

The relative velocity is, of course, either a function of laboratory (impact) energy divided by projectile mass or of relative energy divided by reduced mass. The implicit equation for R_x is

$$e^2(R_x^{-1} + AR_x^{-4}) = \Delta E/(z-1) ,$$

where A is the appropriate polarization coefficient. The parameter $\Delta E/(z-1)$ implies an R_x, which gives the magnitude of σ^{LZ} and, through the function $\Delta U_x(R_x)$, also gives ΔU_x and, hence the velocity position of σ^{LZ}. Figure 3 is a series of such σ^{LZ} cross sections, using the target polarizability of Ne and a velocity scale convenient for $z = 4$. The velocity for which σ^{LZ} is a maximum is determined from Eq. (4.4), which gives

$$(z-1)V_R^M = 81.0 \left(\frac{\Delta U_x}{\Delta E/(z-1)} \right)^2 (1+\mu)^{-1} (10^7 \text{ cm/sec}) . \qquad (4.5)$$

Since $\Delta U_x(R_x)$ is very roughly proportional to e^{-aR_x} and $\Delta E/(z-1) \propto R_x^{-1}$, we have $(z-1)V_R^M \propto R_x^{-2} e^{-2aR_x}$. The trends of the magnitude and velocity position of σ^{LZ} as a function of R_x are thus apparent.

The applicability of these σ^{LZ} functions is of

course subject to the validity of the LZ theory itself as well as to the accuracy of the chosen $\Delta U_x(R_x)$ function for all systems. In particular, we note that the theory is strictly valid only for one-electron transitions between s states and does not include the effects of transitions away from the crossing region.[4] Nevertheless, this σ^{LZ} function is a useful guide to the cross section expected on the basis of the LZ theory and will be referred to in Sec. V.

V. RESULTS AND DISCUSSION

In this section the measured cross sections will be considered in detail. The relative collision velocity V_R is the natural parameter for comparison of results, since it is intrinsic to the impact-parameter separation of nuclear and electronic motions, upon which the LZ and other low-velocity treatments of atomic collisions are based. Therefore, all cross sections are plotted as a function of V_R.

From a comparison between the magnitude and shape of the measured cross section and the approximate cross sections expected for particular interacting states, inferences can be made about the final states and processes likely to be involved. Each combination of projectile and target has a unique set of states. In most cases, more than one pair of states are sufficiently close in energy during part or all of the collision for transitions to be possible. Therefore, interpretation of results requires consideration of all pertinent states. If only the ground states are considered, similar results might be expected for single-electron capture by C^{4+} from He, Ne, and Ar, since the respective energy defects are 39.9, 42.9, and 49.7 eV. However, the experimental cross section for Ar is much larger and varies less as a function of relative velocity.

The presence of an appreciable number of metastable excited ions in the projectile beam of C^{4+} is unlikely because they have a very high excitation energy ($\geq$ 298 eV) compared to the fourth ionization potential ($IP_4 = 64.5$ eV) of carbon, and the source output of C^{5+} ($IP_5 = 392$ eV) is much less than that of C^{4+}. Since the final ion states are undetermined, the measured cross section includes any contributions from single-electron capture with target excitation or ionization, in addition to simple single-electron capture into the ground or excited states of C^{3+}.

A. Carbon (4+) on Helium and Neon

The experimental results are given in Fig. 4. For He, the curve through the points consists of two linear segments, which are least-squares fits, and a smooth curve joining them. For Ne, the curve is a polynomial fit of degree 3 in velocity.

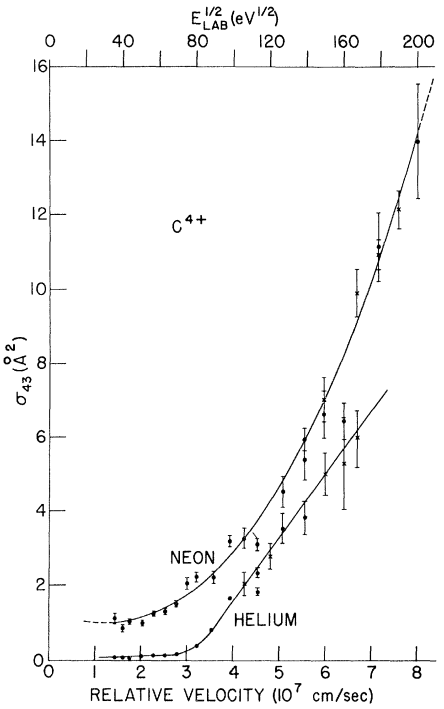

FIG. 4. Total single-electron capture cross sections by C^{4+} in He and Ne.

Each point was weighted in the curve fits in inverse proportion to its deviation σ_s.

Helium as a target gas has several features that distinguish it from other rare gases. Both of its electrons are in s states; therefore, if capture is into an s state, the transition is between spherically symmetric states, to which most theoretical treatments have been restricted. The excitation energies of He^+ are large ($\geq$ 40.8 eV), so that single-electron capture with target excitation is endothermic for $IP_x < 65.4$, as it is for capture by C^{4+}; therefore, capture into the ground or excited states of C^{3+} without target excitation are the only exothermic possibilities to be considered for He.

The interactions of C^{4+} with Ne and with He are similar in that their respective crossing points for single-electron capture are in the same ranges. The ionization potential of Ne is smaller than that of He so that the energy defects are larger. Consequently, the respective crossing points are at somewhat smaller R. Since the outer electrons of Ne are in p states, most of the transitions to be considered are not s-s transitions.

Table II lists the exothermic states to be considered along with the LZ parameters obtained according to Sec. IV. As noted, these are all the exothermic states for the He case. However, the excitation energies of Ne^+ are sufficiently small ($E_{ex} \geq 26.9$ eV), so that single-electron capture into the $2s$ (or $2p$) state of C^{3+} with target excitation is ex-

TABLE II. States and parameters for single-electron capture.

System	Projectile Initial config.	Projectile final config.	Final excit. energy (eV)	Energy defect ΔE (eV)	Crossing point R_x (a_0)	LZ parameters $\Delta U_x(R_x)$ (eV)	LZ parameters σ_{max}^{LZ} (Å^2)	LZ parameters V_R^M (10^7 cm/sec)	Target excitation ΔE max (eV)	Target excitation R_x min (a_0)	Target ionization ΔE (eV)	Target ionization R_0 (a_0)
C^4+He	$1s^2$	$2s$	0	39.9	2.51	6.71	2.5	5.4	−0.9	···	−14.5	···
		$2p$	8.0	31.9	2.93	5.03	3.4	5.0	−8.9	···	−22	···
		$3s$	37.5	2.36	34.6	$<10^{-9}$	large	small	−38.4	···	−17	···
		$3p$	39.7	0.23	362	$<10^{-9}$	large	small	−40.6	···	−54	···
		$3d$	40.3	−0.37	···	···	···	···	−41.2	···	−55	···
C^4+Ne	$1s^2$	$2s$	0	42.9	2.63	6.17	2.8	3.8	16.0	5.3	1.8	88.3
		$2p$	8.0	34.9	2.97	4.89	3.5	3.7	8.0	10.2	−6.1	···
		$3s$	37.5	5.38	15.2	0.0003	large	small	−21.5	···	−35.7	···
		$3p$	39.7	3.25	25.1	0.0002	large	small	−23.7	···	−37.8	···
		$3d$	40.3	2.65	30.8	$<10^{-9}$	large	small	−24.3	···	−38.4	···
$C^{4+}+Ar$	$1s^2$	$2s$	0	48.7	3.19	4.19	4.1	1.4	35.3	3.7	21.1	7.96
		$2p$	8.0	40.7	3.44	3.55	4.8	1.4	27.3	4.2	13.1	12.5
		$3s$	37.5	11.2	7.76	0.29	25	0.15	−2.3	···	−16.4	···
		$3p$	39.7	9.1	9.34	0.09	72	0.02	−4.4	···	−18.6	···
		$3d$	40.3	8.45	9.95	0.061	179	0.01	−5.0	···	−19.2	···
		$4s$	49.8	−1.03	···	···	···	···	−14.5	···	−28.7	···
$C^{2+}+Ne$	$2s^2$	$2p$	0	2.82	9.71	0.072	38	0.053	−24.1	···	−38.3	···
		$2s2p^2$	5.33	−2.51	···	···	···	···	−29.4	···	−43.6	···

othermic for Ne; the corresponding crossing points are in, and above, the intermediate range ($R_x^{ex} \geq 5.3a_0$). In fact, capture ionization, in which a second electron is excited to the continuum, is also exothermic for Ne and will be discussed in relation to the Ar results. Capture ionization is a two-electron process, but capture excitation does not necessarily require a change in state of two electrons. For example, the lowest excited state of Ne^+ is $2s2p$,[6] which results from the removal of a $2s$ electron.

There is not much information on which to assess the contribution of capture excitation to the Ne cross section. Other results[22] show that target excitation does occur in low-velocity collisions. Collisions that excite the Ne^+ may very well be part of the measured cross section, in particular, at low velocities. However, the similarity between the Ne results and the He results, for which target excitation is endothermic, suggests that most of the cross section is simple electron capture.

Specific calculations of the transition probabilities for these ion-atom combinations have not been made. However, let us consider the empirical σ^{LZ} of Sec. IV. Capture into the $n=2$ states with close crossings has a very broad σ^{LZ} with little similarity to the measured cross sections. Capture into the $n=3$ states with distant crossings is beyond the range of application of the LZ calculations, but extrapolation would indicate a large peak at very low velocities.

As previously mentioned, BJS have obtained a very interesting result for a process ($Mg^{2+}+H \rightarrow Mg^+ + H^+ + 1.4$ eV) with a distant crossing at $R_x = 18.9a_0$. The active electron is captured from the $1s$ state of H into the $3s$ state of Mg^+. Their result has a second maximum at higher velocity than the LZ maximum and, according to BJS, is due to transitions that occur in the range of R of order $\frac{1}{2}R_x$. For moderate R_x this contribution from transitions occurring away from the crossing point is merged with the ordinary LZ-type contribution from transitions near the crossing point. The theoretical trend of the position of the second maximum is toward higher velocities for larger crossing points.

Similar results should be expected for the $1s$ to $3s$ transition in both $C^{4+}+He$ and $Mg^{2+}+H$, since the theoretical treatment considers one active electron outside a closed shell and neglects interactions with other electrons. These results are compared in Fig. 5 as a function of V_R without normalization.

The $C^{4+}+He$ system also has a potential curve for capture into the $3p$ state which is exothermic by only 0.37 eV and lies about 2 eV above the $3s$ state throughout the interaction. Capture into the $3p$ state might be part of the measured cross section; however, p states have not been treated theoretically and the relative $3p$-versus-$3s$ contribution is unknown. In view of the experimental limit of error and the similarity of the two systems, the closeness of the cross sections must be considered somewhat fortuitous. However, we conclude that the measured

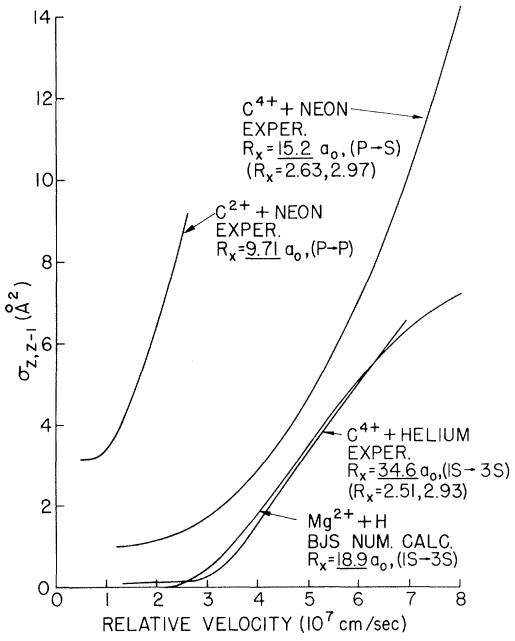

FIG. 5. Single-electron capture cross sections for systems with distant crossings.

C^{4+} + He cross section is a BJS second maximum due to capture into the states with distant crossings. The C^{4+} + Ne states have been reviewed above, and a similar conclusion is made.

Included in Fig. 5 are results for C^{2+} + Ne ($R_x = 9.7a_0$ for $2p \rightarrow 2p$) also obtained with the present apparatus using an electron-impact ion source. The C^{2+} + Ne results have the same shape but are smaller than previously reported values.[23] If the C^{2+} is in the ground state, the only crossing is at $9.7a_0$. Capture into any other state is endothermic by ≥ 24 eV. A portion of the C^{2+} ions might be $2s2p$ metastables, for which there are additional crossings. However, assuming the C^{2+} ion to be predominately ground state also allows this cross section to be interpreted as a second maximum.

B. Carbon (4+) on Argon

The experimental results are given in Fig. 6, where the smooth curve is a polynomial fit of degree 2, weighted in inverse proportion to the σ_s of each point. This total cross section is more than 50 times those for He and Ne.

The analysis of the exothermic states in this case is more complex. First we consider single-electron capture without target excitation, which is exothermic for the same set of final states as Ne (Table II). Since the first *IP* of Ar is smaller (Table III), the ΔE are larger and the R_x tend to be smaller. The R_x for $n = 2$ states are also very close, but slightly more distant because of a larger polarization term. The R_x for the $n = 3$ states are much smaller, but still distant enough to have σ^{LZ} maxima at small $V_R \leq 0.15 \times 10^7$ cm/sec. Suppose the $\Delta U_x(R_x)$ parameter were larger by as much as a factor of 4. Then the σ^{LZ} maximum for the $3s$ state would be at 2.4×10^7 cm/sec, but would be only one-half the magnitude of the experimental results. There may also be some contribution due to second-maximum-type transitions. However, if the LZ theory is assumed approximately valid, then single-electron capture alone does not account for the magnitude of the measured cross section throughout the velocity range.

There is a significant difference of the Ar target in regard to target excitation and ionization, which will be discussed below. First, let us note the effective radius of a sphere within which the interaction must occur to produce a cross section of 50 Å^2, using $\sigma = \pi R_e^2 P(V_R)$. Taking the process to be reversible with a maximum probability of $\frac{1}{2}$, gives $R_e = 10.6a_0$, whereas taking it to be irreversible with a maximum probability of 1, gives $R_e = 7.5a_0$. In either case, an interaction at moderate to large R is implied by the results.

C. Capture Ionization

Capture ionization [Eq. (1.2)] is an Auger process in which one electron is captured and a second electron is ejected to the continuum by receiving some at the excess potential energy[24,25] defined as $\Delta E = (IP_z)_P - (IP_1 + IP_2)_T$, where z is the initial projectile charge. Although capture ionization by C^{4+} is exothermic for both Ne and Ar targets ($\Delta E = 1.8$

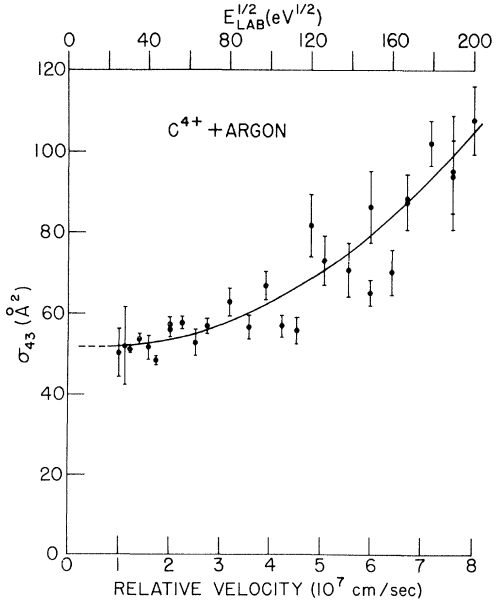

FIG. 6. Total single-electron capture cross section by C^{4+} in Ar.

TABLE III. Ionization potentials (eV).

	IP_1	IP_2	IP_3	IP_4	IP_1+IP_2
C	11.27	24.38	47.88	64.49	35.6
He	24.59	54.41			79.0
Ne	21.56	41.08	63.70	97.18	62.6
Ar	15.76	27.62	40.91	59.81	43.4
H	13.60				
Mg	7.65	15.03	80.13	109.3	22.7

and 21.1 eV, respectively), an examination of the potential curves below reveals an essential difference.

Kishinevskii and Parilis[25] noted that capture ionization can occur via three channels: (a) directly, where one electron is captured and another is simultaneously ejected from the target; (b) by single-electron capture into an excited state, which then interacts with the target to eject a second electron; (c) by two-electron capture into a doubly excited state, which auto-ionizes during or after the collision. The first two of these may be viewed as an auto-ionization of the quasimolecule. In channel (a) there is a direct interaction with a continuum of states having positive electron energy (E_k), whereas the other two channels are two-stage processes, the first stage being an interaction between discrete states at a pseudocrossing. Kishinevskii and Parillis calculated cross sections for these three channels by using LZ probabilities for the discrete-state interactions, by assuming the pseudocrossings can be treated independently, and by calculating Auger ionization probabilities for the discrete-continuum interactions.

Considering capture excitation, in contrast to capture ionization, we note that, for most final excited states of the target ion, capture excitation is conceptually the same two-electron process as capture ionization, but has discrete final states. An exception to this, which is a one-electron process, corresponds to the excited target state resulting from the removal of an inner electron, e.g., the lowest excited state of Ne^+ (or Ar^+) is caused by the removal of a $2s$ (or $3s$) electron. Another difference is that capture excitation is reversible with a maximum average probability of $\frac{1}{2}$, whereas capture ionization is irreversible, in a given collision, with a maximum average probability of 1.

Approximate pseudocrossing curves for the C^{4+} + Ar system are shown in Fig. 7. The initial curve includes only the R^{-4} polarization of Ar; the final curves include the R^{-1} Coulomb term and are displaced by the exothermic energy defects. The lowest solid curve is for capture into the $2s$ ground state of C^{3+} without excitation of Ar^+. There is a set of curves above these, including many in the cross-hatched region, for which Ar^+ is excited and also a continuum of curves for capture ionization. The boundary of the continuum corresponds to $E_k = 0$, and R_0 is the point where it crosses the initial

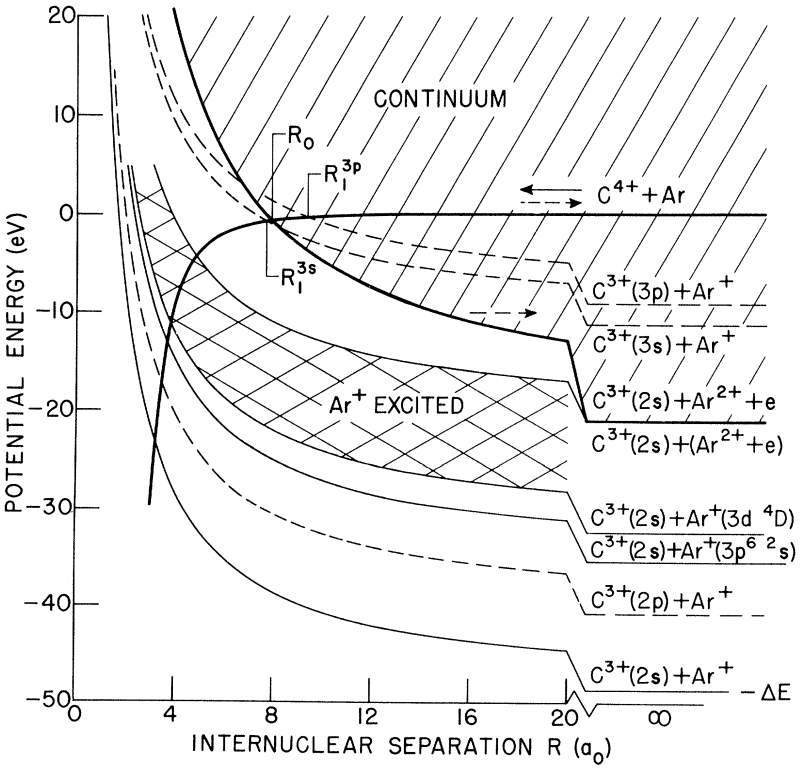

FIG. 7. Approximate diabatic potential curves for C^{4+}+Ar.

curve. The lowest dashed curve is for capture into the $2p$ state of C^{3+} without excitation of Ar^+, and the corresponding curves for excited and ionized Ar^+ lie above the respective $2s$ curves by 8.0 eV, but are not shown. The other two dashed curves are for capture into the $3s$ or $3p$ state of C^{3+} without excitation of Ar^+, and R_1 are the points where they cross the initial curve (not shown is the $3d$ curve, 0.6 eV above the $3p$ one). Also not shown are final curves for two-electron capture into auto-ionizing levels of C^{2+}, the lowest of which is a $2p4d$ level with a crossing at $R_2 = 5.3a_0$. Higher levels produce a series of larger R_2, e.g., $2p7p$ gives $R_2 = 7a_0$. The crossings R_1 and R_2 are for channels (b) and (c), respectively. There are, of course, additional states of the quasimolecule $(C + Ar)^{4+}$ above the ones shown, but their wide separation from the initial curve implies little interaction with it.

We note that the obvious condition requiring R_0 to be of order the atomic dimensions to have appreciable interaction is satisfied for Ar ($R_0 = 8a_0$) and hence, direct Auger ionization should be probable. In contrast, we find $R = 88a_0$ for Ne, and since little interaction can be expected at such a large distance, Auger ionization is improbable. In terms of the potential curves, channel (a) requires an interaction between the initial curve and the continuum states, channel (b) requires an interaction at $R_1(3s)$ or $R_1(3p)$ and subsequent interaction with the continuum, and channel (c) requires an interaction at R_2 and subsequent auto-ionization of the doubly excited C^{2+} atom. Since we have $R_0 \approx R_1 \approx R_2$, it is not possible to treat the channels separately. Also, any treatment of individual crossings is subject to the BJS results that transitions are probable not only in the crossing region. However, since channel (a) does not depend upon crossing of discrete states, it is more likely to be dominant over a wide range of velocities. Finally, we note that taking an effective radius of $R_e = R_0 = 8a_0$ and a transition probability of 1 is consistent with the experimental results for $C^{4+} + Ar$, as noted in Sec. V B.

Complementary evidence for capture ionization has been provided by the results on total ionization cross sections of Flaks, Ogurtsov, and Fedorenko[26] for $Ne^{z+} + Xe$ where $z = 3, 4$ in contrast to $z < 3$, and by the analysis[25] of those results. Additional information is given by the results of Latypov *et al.*[27]

In regard to capture ionization in general, if the projectile recombination energy is sufficiently large, more than one free electron could be ejected. Since free electrons are produced and the expected cross sections are very large even at low velocities, capture ionization may be an important process in nonequilibrium plasmas.

VI. CONCLUSIONS

The results presented here indicate the importance of considering the effect of transitions away from the pseudocrossing region. In particular, for large R_x, the effect of these transitions produces a cross-section maximum well separated from the predicted LZ maximum, which is at too low a velocity for observation. The LZ theory is most appropriate for moderate R_x, but the precise validity of the theory in this region remains to be determined. Evidence for the large probability of the capture-ionization process under certain conditions is given by the $C^{4+} + Ar$ single-electron capture results.

ACKNOWLEDGMENTS

The support and advice of Professor T. D. Wilkerson is gratefully appreciated. Suggestions about equipment design by E. Grossenbacher and the craftsmanship of his staff were very valuable to the construction of the apparatus.

---

*Work supported by the National Aeronautics and Space Administration, under Grant No. NsG-283, the National Science Foundation, under Grant No. NSF-8325, and by the Board of Regents of the University of Maryland.

[1]J. V. Neumann and E. Wigner, Z. Physik 30, 467 (1929).

[2]J. B. Hasted and A. Y. J. Chong, Proc. Phys. Soc. (London) 80, 441 (1962).

[3]J. B. Hasted and M. Hussain, Proc. Phys. Soc. (London) 83, 911 (1964).

[4]D. R. Bates, Proc. Roy. Soc. (London) A257, 22 (1960); see also D. R. Bates, in *Atomic and Molecular Processes*, edited by D. R. Bates (Academic, New York, 1962).

[5]J. Heinrichs, Phys. Rev. 176, 141 (1968).

[6]D. R. Bates, H. C. Johnson, and L. Stewart, Proc. Phys. Soc. (London) 84, 517 (1964).

[7]H. J. Zwally, David W. Koopman, and T. D. Wilkerson, Rev. Sci. Instr. 40, 1492 (1969).

[8]H. J. Zwally, Ph.D. thesis, University of Maryland Technical Note No. BN-582, 1968 (unpublished).

[9]J. Mattauch, Phys. Rev. 50, 617 (1936).

[10]Varian Associate 10-cm magnet with Fieldial power supply.

[11]Varian Associates, Palo Alto, Calif.

[12]MKS Instrument Inc., Burlington, Mass.

[13]Micro Instrument Co., Gardena, Calif.

[14]H. Jay Zwally, Rev. Sci. Instr. 41, 1489 (1970).

[15]N. G. Utterback and T. Griffith, Jr., Rev. Sci. Instr. 37, 866 (1966).

[16]D. R. Bates and B. L. Moseiwitsch, Proc. Phys. Soc. (London) 67, A805 (1954).

[17]A. Dalgarno, Proc. Phys. Soc. (London) 67, A1010 (1954).

[18]D. R. Bates and J. T. Lewis, Proc. Phys. Soc. (London) 68, A173 (1955).

[19]D. R. Bates and T. J. M. Boyd, Proc. Phys. Soc. (London) 69, A910 (1956).

[20]T. J. M. Boyd and B. L. Moisewitsch, Proc. Phys. Soc. (London) 70, A809 (1957).
[21]B. L. Moisewitsch, J. Atmospheric Terres. Phys. Suppl. 2, 23 (1955).
[22]M. Lipeles, R. Novik, and N. Tolk, Phys. Rev. Letters 15, 815 (1965).
[23]J. B. Hasted and R. A. Smith, Proc. Roy. Soc. (London) A235, 354 (1956).
[24]L. M. Kishenevskii and E. S. Parilis, in *Proceedings of the Fifth International Conference on the Physics of Electronic and Atomic Collisions* (Nauka, Leningrad, 1967), p. 100.
[25]L. M. Kishenevskii and E. S. Parilis, Zh. Eksperim. i Teor. Fiz. 55, 1932 (1969) [Soviet Phys. JETP 28, 1020 (1969)].
[26]I. P. Flaks, G. N. Ogurtsov, and N. V. Fedorenko, Zh. Eksperim. i Teor. Fiz. 41, 1438 (1961)[Soviet Phys. JETP 14, 1027 (1962)].
[27]Z. Z. Latypov, N. V. Fedorenko, I. P. Flaks, A. S. Shaporenko, in *Proceedings of the Sixth International Conference on Physics of Electronic and Atomic Collisions* (M.I.T. Press, Cambridge, Mass., 1969), p. 1010.

PHYSICAL REVIEW A VOLUME 2, NUMBER 5 NOVEMBER 1970

Generalized Variational Bounds on the Positron-Hydrogen Reaction Matrix. I. The Coupled-Static Approximation

Johan F. Dirks*† and Yukap Hahn
Department of Physics, University of Connecticut, Storrs, Connecticut 06268
(Received 8 April 1970)

The theory of generalized variational bounds is applied to two-channel collisions of positrons on hydrogen leading to positronium formation. The formalism is developed in detail for this problem, and the zero partial-wave solution is obtained in the coupled-static approximation. The nonlocal coupling kernels and the behavior of the wave functions are exhibited in detail. Eigenphase shifts and coupling parameters, and the stripping and pickup cross sections, as well as the elastic amplitudes for positron-hydrogen and positronium-proton collisions, are studied as functions of scattering energies. The unitarity limits are exhibited, one of which is nearly saturated in the Ps-p channel. A useful iteration procedure for solving the coupled equations with large coupling kernels is developed.

I. INTRODUCTION

The three-particle problem in quantum-mechanical collision theory has been studied for many years.[1,2] In particular, a formally consistent mathematical procedure has been given by Faddeev[3] and others,[4] but its application to specific physical systems is a much more formidable task.[5,6] When only a few two-body channels are open, however, a theoretically more tractable procedure is available in the form of the generalized variational bounds[7] (GVB). It correctly treats the nonorthogonality problem of the rearrangement channels, and the effect of distortions due to coupling to other closed channels is estimated variationally with the strong *bound* property. The theory is essentially of the same degree of applicability for the low-energy scattering problem as the Ritz variational principle is for the bound-state problems. Its earlier version[8] has been applied to the elastic positron-hydrogen scattering[9] and elastic electron-hydrogen scattering,[10] where the simple channel projection operators are explicitly available.[11] The result gave a valuable insight into the effect of distortions on the scattering parameters and also on the resonance structures.[12]

This is the first of a series of reports on the detailed theoretical analysis of the positron-hydrogen scattering system, using the formalism of GVB. By restricting the scattering energies to the region below the first excitation threshold in the positron-hydrogen channel (channel 1) but above the positronium-proton elastic threshold (channel 2), we have probably the simplest two-channel scattering problem in which rearrangement of the electron takes place as

$$\underset{\text{channel 1}}{e^+ + (e^- + p^+)} \rightleftharpoons \underset{\text{channel 2}}{(e^+ + e^-) + p^+} \quad . \tag{1.1}$$

The effect of the coupling to the electromagnetic field may be neglected, and the ability to distinguish between the two light particles and the very heavy proton core simplifies the analysis to a manageable level with the computers available at present. Because of complicated nonorthogonality between the two open-channel wave functions, no simple channel projection operators of the Feshbach type[13] are available, and GVB, which explicitly avoid such a requirement, can thus be effectively applied to this problem.

The reaction (1.1) has been studied many times